SAND2015-1898C

Process modeling and experiments for forging and welding*

**Arthur A. Brown, Lisa A. Deibler, Lauren L. Beghini,
Timothy D. Kostka, and Bonnie R. Antoun**

**Sandia National Laboratories, Livermore, CA 94551
aabrown@sandia.gov**

ABSTRACT

We are developing the capability to track material changes through numerous possible steps of the manufacturing process, such as forging, machining, and welding. In this work, experimental and modeling results are presented for a multiple-step process in which an ingot of stainless steel 304L is forged at high temperature, then machined into a thin slice, and finally subjected to an autogenous GTA weld. The predictions of temperature, yield stress, and recrystallized volume fraction are compared to experimental results.

Keywords: modeling, forging, welding, microstructure, recrystallization

Introduction

The microstructure and properties in mechanical components are highly sensitive to the processing conditions under which the component is manufactured. The ability to predict the evolution of material properties during thermal-mechanical processing can be valuable in component design. Process conditions can be optimized to achieve desirable yield stress, microstructure, and residual stress. To this end, we are developing the capability to track material changes through numerous possible steps of the manufacturing process, such as forging, machining, and welding. In this work, experimental and modeling results are presented for a multiple-step process in which an ingot of stainless steel 304L is forged at high temperature, then machined into a thin slice, and finally subjected to an autogenous gas tungsten arc (GTA) weld. The predictions of temperature, yield stress, and recrystallized volume fraction are compared to experimental results.

Material model

A treatment of the kinematics and thermodynamics of the material model utilized in the simulations presented here is documented in [1]. The internal state variable model accounts for rate and temperature dependence, and tracks the evolution of static and dynamic recrystallization. The model was validated in [2], where it was demonstrated to accurately predict the final yield strength at multiple locations in forgings of different geometries and forging temperatures. In this work, the same material parameter set is used as in [2].

Experiments and simulations

* This work was performed at Sandia National Laboratories. Sandia is a multiprogram laboratory operated by Sandia Corporation, a Lockheed Martin Company, for the United States Department of Energy under contract DEAC04-94AL85000.

Forging

A cup-shaped forging from 304L stainless steel was produced using four forging stages, where the final stage was performed at 829 °C (1525 °F) and was preceded by a furnace anneal at 982 °C (1800 °F) and a flattening operation at 816 °C (1500 °F). For the purposes of modeling, it was assumed that the annealing removed the effects of the previous stages, so only the flattening and the final forging stage were simulated (see Figure 1). The thermal and mechanical codes used are part of Sandia's Sierra Multiphysics Code (see [3] and [4]). The simulations include the effects of furnace heating, die chill, radiation, convection, and heat generation due to plastic dissipation. It is assumed that 95% of the plastic work is dissipated as heat.

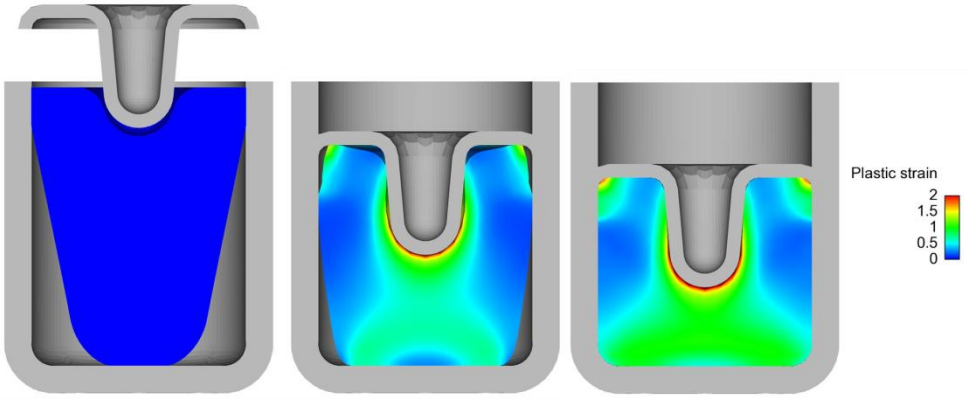

Fig. 1 The simulated evolution of plastic strain during the flattening operation and the final forging stage

In order to obtain microstructures for as-forged and post welded that could be reasonably compared, the forging was cut in half along the vertical axis, then quarter inch slices were cut from each half. The U-shaped slices were then cut along the mirror axis of the U (Figure 2) and two of the mating surfaces were used to investigate the changes in microstructure and hardness in the heat affected zone.

Welding

An autogenous gas tungsten arc weld was performed on one side of one of the forging slices. Eight thermocouples were spot-welded in various locations on both the front and back surface of the forging slice (Figure 2). The slice was supported by a thin metal frame to raise the sample off of the backing plate and provide room for the thermocouples on the back of the part (Figure 3). Tabs were spot welded on to the top and bottom of the slice to avoid the effects of starting and stopping the weld on the heat affected zone in the part. The whole assembly was clamped into a fixture, and a GTA weld was performed at 130 A, travel speed 2.5 inches per minute.

For the modeling of the welding process, the tabs and the clamping shims were included. The stress state and internal state variables were mapped from the forged mesh to the mesh used for the welding simulation using Exomerge [5]. Figure 8 shows the temperature contour in the specimen and tabs during the simulation. The heat flux input to the top surfaces of the tabs and forged specimen was optimized to get the simulation temperature histories at the thermocouple locations to match the experimentally measured histories (Figure 8). Only data from the first five thermocouples was obtained, and the experimental output from thermocouple 4 is not accurate after the peak temperature since the torch knocked off the thermocouple shielding as it passed by. A fairly good representation of the thermal histories is obtained through the simulation of the welding process

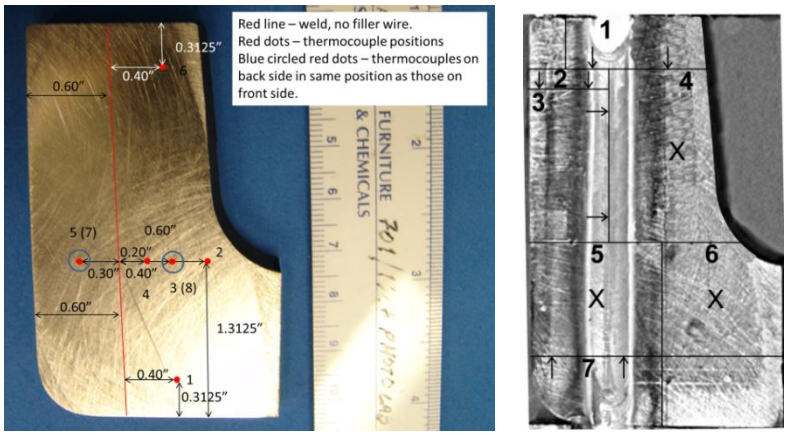

Fig. 2 The slice before welding with locations of the thermocouples indicated (left image). A map of the metallographic sections on the welded part is shown on the right. Planar sections are indicated by X, transverse or longitudinal sections are arrowed to indicate the face mounted. The as-forged part was cut similarly.

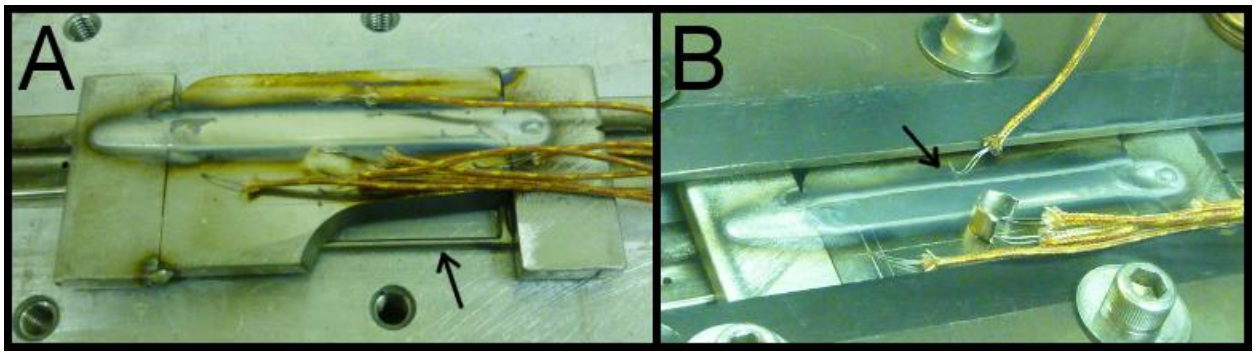

Fig. 3 The welded part, showing the start and stop tabs at each end of the weld and the support framework (left image). The part was clamped during welding (right image)

Measurements of recrystallized volume fraction and hardness

Both the welded and the un-welded pieces were sectioned for metallography, as shown in Figure 2. Samples were polished to a 0.3 micron finish. Hardness testing was performed on polished samples. Vickers hardness testing was performed with 100 gm load, and 15s dwell time, keeping track of the X and Y position of each indent. In order to compare with the modeling results, the Vickers hardness needed to be converted to yield strength. A conversion between Knoop hardness and yield strength was available from [6]:

$$\sigma_y = 2.673 \cdot 10^6 HK - 1.489 \cdot 10^8 \text{ Pa} \tag{1.1}$$

The following conversion between Vickers and Knoop hardness was obtained by performing ten measurements of each type on forging specimens subjected to various heat treatments to achieve various hardness values:

$$HK = 1.115 HV - 9.801 \tag{1.2}$$

The above two equations were used to convert the Vickers hardness measurements to yield strength (Figure 4). The yield strength derived from this calculation is plotted in Figures 7 and 10 for the as-forged and as-welded specimens. The markers indicate where data was collected.

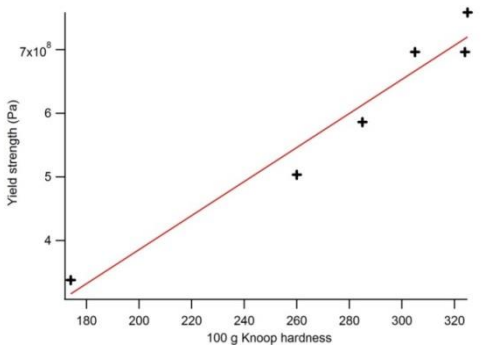

Fig. 4 Data to establish conversion between Knoop hardness and yield strength

After hardness testing was complete, samples were etched for microstructural imaging with 60% HNO_3, 40% DI H_20 electrolytic at 1.5 volts for 20-60 seconds (ASTM E407-219). Optical micrographs were taken at regular intervals on both sets of samples, keeping track of the position of each micrograph. At each location where recrystallization data was desired, three separate fields of view were captured to allow for statistical analysis of data. The amount of recrystallization was determined by visually defining which grains appeared recrystallized (generally smaller with a rounder outline) and measuring the volume fraction of recrystallized material using Clemex image analysis tool (see Figure 5).

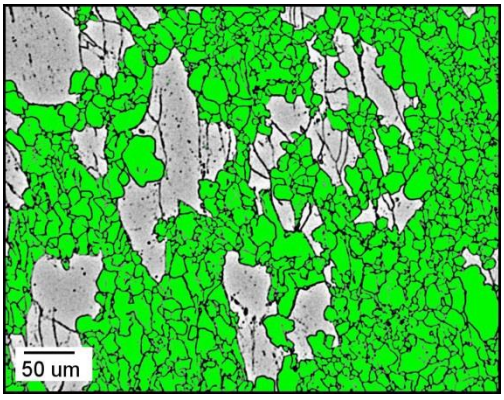

Fig. 5 An example of the microstructure imaging used to determine the recrystallized volume fraction. This image came from the as-forged condition (bottom-right of section 6), with measured values of 48% recrystallization and 233 Vickers hardness.

Results

The results of the recrystallized volume fraction measurements for the forged specimen before the welding operation are plotted in Figure 6, and the results corresponding to the specimen after welding are shown in Figure 9. Individual data points are marked in the figure; the color map is an extrapolation between data points. The average standard deviation of the non-zero or one-hundred percent recrystallization measurements is ± 3%. Because of the size of samples for metallographic sectioning, the entire area of the forging could not be evenly sampled. The model predictions of the recrystallized volume fraction are also shown in Figures 6 and 9. The simulations predict that the forging process alone leads to almost complete recrystallization right under the punch. The general trends are consistent, in that both the experiments and the simulations show significant recrystallization on the sidewalls and bottom of the inner forging surface, where the punch produced the highest plastic strains in the forging (Figure 1).

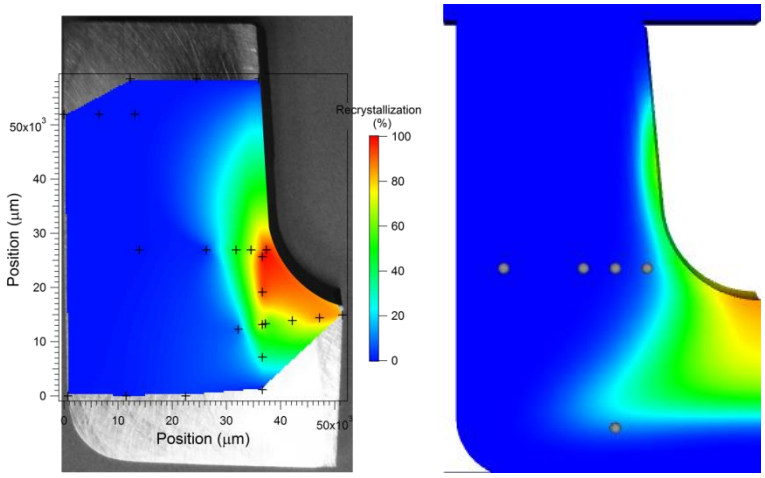

Fig. 6 The measured (left) and predicted (right) recrystallized volume fraction before the welding operation

The model prediction of the as-forged yield stress is shown in Figure 7. The highest strength is at the bottom of the specimen. This is due to die chill; the bottom is cooled due to conduction to the die, and thus is plastically deformed at a lower temperature, which leads to more stored energy in the dislocation structure. The strength is predicted to be low under the punch, due to the recrystallization that wipes away the dislocation structure there, softening the material. This effect is not evident in the experimental results. It is not clear to the authors why the measured yield stress is high in some locations that exhibited significant recrystallization. This will be further investigated in the future through additional measurements. There are obviously some artificial artifacts due to the interpolation between experimental measurements that is used to create the experimental contour plots. (In fact, Figure 10 shows that the experimental results in the as-welded sample do exhibit low yield stresses under the punch, which we do not believe is due to the weld.)

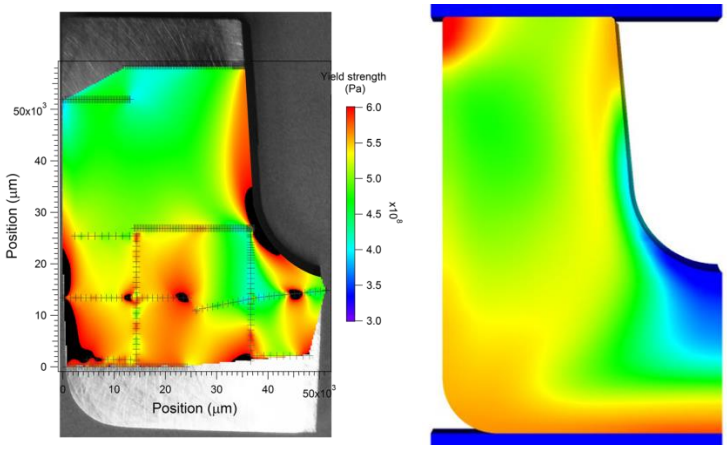

Fig. 7 The measured (left) and predicted (right) yield strength of the forging before the welding operation

The autogenous weld that travels up the specimen sidewall introduces high local temperatures, which leads to melting and solidification, as well as a heat-affected zone that experiences recrystallization and softening (Figures 9 and 10). The model in its current form does not account for melting and solidification, but as can be seen in the figures, does predict the recrystallization and local softening in the weld region and heat-affected zone.

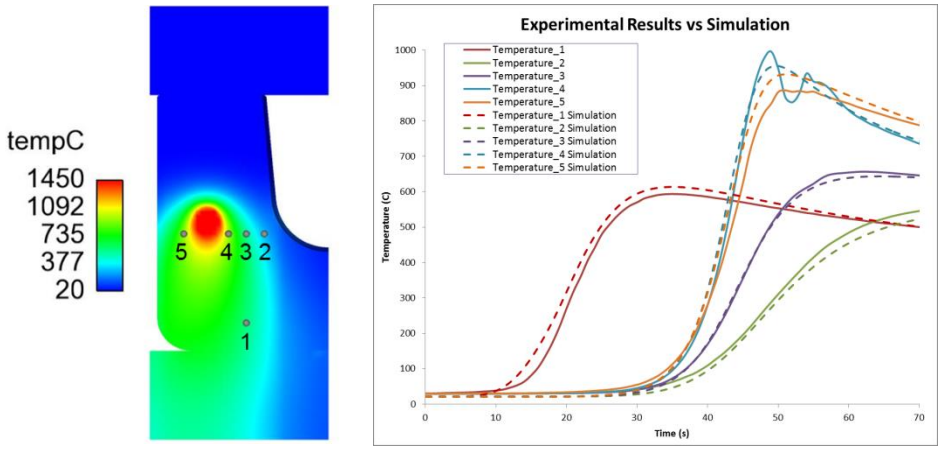

Fig. 8 The temperature profiles from the thermocouples. The simulation temperatures at the same locations are shown for comparison

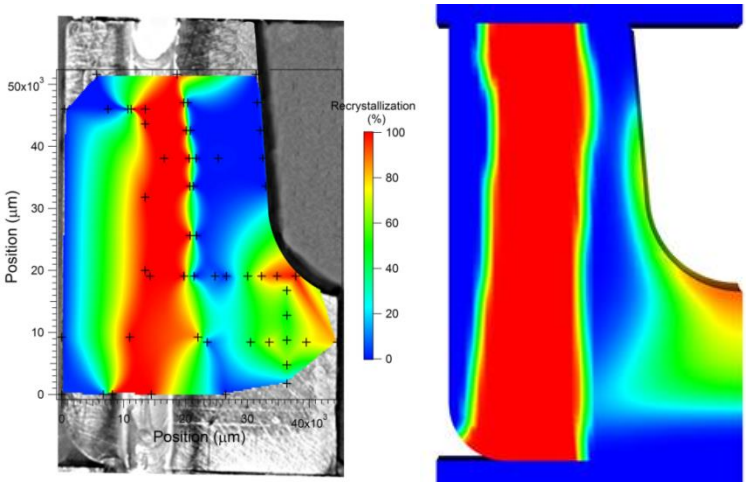

Fig. 9 The measured (left) and predicted (right) recrystallized volume fraction after the welding operation

Uncertainty quantification will be performed as future work. The predictions of room temperature yield stress and recrystallized volume fraction are very sensitive to certain simulation inputs, such as the time it takes to get the forging out of the die and into the quench bath. The results presented here are for nominal input values, but future work will be to include the effects of uncertainties on the final predictions.

Conclusions

This paper demonstrates the capability to model multiple stages of manufacturing processes such as forging and welding. There are some discrepancies between predictions and experimental measurements that still need to be addressed, but the general trends of recrystallization and softening are captured in the as-forged and as-welded specimens.

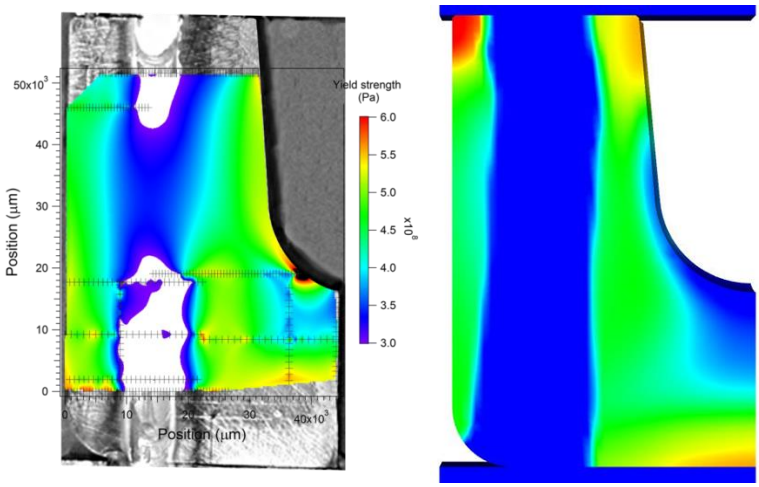

Fig. 10 The measured (left) and predicted (right) yield strength of the forging after the welding operation

[1] Brown, A.A. and Bammann, D. J. "Validation of a model for static and dynamic recrystallization in metals," International Journal of Plasticity, Vol. 32-33, pp. 17-35, 2012.

[2] Brown, A.A., Kostka, T.D., Antoun, B.R., Chiesa, M.L., Bammann, D.J., Pitts, S.A., Margolis, S.B., O'Connor, D., and Yang, N.Y.C. "Validation of Thermal Mechanical Modeling for Stainless Steel Forgings," COMPUTATIONAL PLASTICITY XI: FUNDAMENTALS AND APPLICATIONS, Pages: 1153-1164, 2011.

[3] SIERRA Solid Mechanics Team. Adagio 4.14 User's Guide. Sandia Report 2009-7410, 2009.

[4] Notz, P.K., Subia, S.R., Hopkins, M.M., Moffat, H.K., and Noble, D.R. Aria 1.5 User Manual. Sandia Report 2007-2734, 2007.

[5] Kostka, T.D., "Exomerge User's Manual: A lightweight Python interface for manipulating Exodus files", SAND2013-0725, 2013.

[6] Robinson, S., and Story, C. Unpublished data for converting Knoop hardness to yield stress for 304L stainless steel.